

Facile synthesis of two-dimensional highly branched gold nanostructures in aqueous solutions of cationic gemini surfactant†

Cite this: *CrystEngComm*, 2013, 15, 2648

Wentao Wang, Yuchun Han, Mingyuan Gao* and Yilin Wang*

Snowflake-like two-dimensional highly branched gold nanostructures (2DHBNs) have been constructed in the presence of hexamethylene-1,6-bis (dodecyl dimethylammonium bromide) ($C_{12}C_6C_{12}Br_2$) through the reduction of $HAuCl_4$ by ascorbic acid. High resolution transmission electron microscopy results indicate that the 2DHBNs are uniform in crystallographic orientation, where the branched nanostructures grow along the $\langle 211 \rangle$ direction and present multiple twin planes stacked along the $\langle 111 \rangle$ direction. An ex situ kinetic study, followed by TEM observations, shows that the 2DHBNs are evolved from triangular nanoprisms through overgrowth along the $\langle 211 \rangle$ direction. The gemini surfactant $C_{12}C_6C_{12}Br_2$ is found to be the most essential factor for the formation of the 2DHBNs. $C_{12}C_6C_{12}Br_2$ may selectively adsorb onto the (111) planes, which promotes the construction of 2D nanostructures. Moreover, $C_{12}C_6C_{12}Br_2$ can act as an excellent kinetic modifier to control the growth of the nanostructures, which also affects the generation of branched nanostructures. The as-prepared 2DHBNs exhibit an efficient surface-enhanced Raman scattering (SERS) property which has potential application in constructing sensitive SERS substrates.

Received 19th September 2012,
Accepted 16th January 2013

DOI: 10.1039/c3ce26527g

www.rsc.org/crystengcomm

Introduction

Two-dimensional (2D) noble metal nanomaterials with one dimension much smaller than the other are a fascinating class of materials with distinct dimension-dependent electronic,¹ plasmonic² and optical properties,³ which have potential applications in sensors,⁴ diagnostics,⁵ photoluminescence,⁶ surface-enhanced Raman scattering (SERS),⁷ catalysis⁸ and so forth. Driven by these intriguing properties and applications, a great deal of effort has been devoted to fabricating various 2D nanomaterials in the form of nanoplates,⁹ nanoprisms,¹⁰ nanodisks¹¹ or nanobelts.¹² In recent years, a new type of 2D nanomaterial, namely 2D highly branched nanomaterials (2DHBNs), has emerged.^{13,14} Compared to non-branched 2D nanomaterials, 2DHBNs have a larger specific surface area and a higher density of edges, corners and stepped atoms on their branches. These characteristics make them ideal candidates for SERS and catalysis.^{15–17} In order to improve the performance of 2D nanomaterials, it is highly desirable to synthesize

2DHBNs with controlled nanostructures to understand the dimension and shape dependent properties.

Due to the highly symmetric face-centered cubic (fcc) structure of noble metal nanocrystals, the fabrication of 2DHBNs with a well-defined hierarchical nanostructure is still a great challenge and the related reports are still limited.¹⁸ To date, interface synthesis, which confines the crystal growth at the air–liquid^{14,19} or liquid–solid^{15,16,20} interface, has been demonstrated to be a feasible approach to construct 2DHBNs. As an example, Pan and co-workers²¹ reported that gold 2DHBNs could be directly formed on TEM sample grids through a seed-mediated method. However, most of the reported 2DHBNs were polycrystalline and often bound to solid substrates, which may restrict their applications in electronics and optics. In addition, the 2D growth carried out on a given surface limits the synthesis efficiency. To develop solution-phase synthetic methods may overcome these disadvantages. Surfactant-assisted syntheses have been considered as an effective method to generate 2DHBNs. Chen and co-workers²² obtained a mixture of gold monopods, bipods, tripods and tetrapods through the reduction of $HAuCl_4$ in the presence of the cationic surfactant cetyltrimethylammonium bromide (CTAB). A high concentration of CTAB was needed to obtain the branched particles and thus the authors suggested that the self-assembled structures of concentrated CTAB might play an important role in the construction of branched shapes. Qi and co-workers^{23a} reported that gold nanocombs could be synthesized in mixed aqueous solutions of CTAB with the

Key Laboratory of Colloid and Interface Science, Beijing National Laboratory for Molecular Sciences (BNLMS), Institute of Chemistry, Chinese Academy of Sciences, Beijing 100190, People's Republic of China. E-mail: yilinwang@iccas.ac.cn; gaomy@iccas.ac.cn; Fax: +86-10-82615802; Tel: +86-10-82615802

† Electronic supplementary information (ESI) available: HRTEM images of typical 2DHBNs and a single arm perpendicular to the TEM grid; SEM images of the gold nanostructures obtained at different reaction times; UV-vis absorption spectra of the 2DHBNs recorded at different times; and TEM image and DLS data of the vesicles formed by $C_{12}C_6C_{12}Br_2$. See DOI: 10.1039/c3ce26527g

anionic surfactant sodium dodecylsulfonate (SDSn). It was proposed that the mixed cationic–anionic surfactants exerted a subtle control over the 2D branched growth of gold nanocrystals due to the cooperative effect of the mixed surfactants. Moreover Qi and co-workers^{23b} found that well-defined 2D gold nanodendrites could be achieved in a mixture of dodecyltrimethylammonium bromide (DTAB) and β -cyclodextrin (β -CD). The formation of supramolecular complexes of DTAB with β -CD was considered to be a prerequisite for the fabrication of the nanodendrites. Tilley and co-workers²⁴ synthesized 2D highly branched palladium nanostructures through their control over the reaction kinetics by varying the ratio of oleylamine and oleic acid. Despite the importance of surfactants, their roles have not been fully elucidated. The most commonly used hypothesis is that surfactants act as capping agents. In this case, surfactants are considered to stabilize the growing nanocrystal and influence crystal habit expression by minimizing otherwise higher energy facets.^{25–27} Furthermore, surfactants always form complexes with metal ions and the complexes can further self-assemble into various aggregates. The formation of complexes and aggregates essentially influences the diffusion kinetics of the metal ions. As a result, the nucleation and growth kinetics of nanocrystals changes simultaneously. In a seed-mediated synthesis,²⁸ the CTA–Au(I) micelles have an extremely low collision frequency with the gold seeds, which causes the growth rate to be retarded by several orders of magnitude. Therefore, the rational modulation of the adsorption and aggregation behavior of surfactants will provide a feasible way to achieve fine control over nanocrystal growth.

Gemini surfactants are constructed from two hydrophobic chains and two polar/ionic head groups covalently connected by a spacer group at the head group level. Due to the special molecular architectures, the aggregates of gemini surfactants have a higher charge density and stronger hydrophobic microdomain compared with the corresponding single chain surfactants.²⁹ As a result, gemini surfactants exhibit a strong adsorption ability at the liquid–solid interface, which makes them excellent capping agents for nanocrystal syntheses.³⁰ Moreover, gemini surfactants can form abundant aggregates at a very low concentration range, including spherical micelles, wormlike micelles, vesicles, lamellar structures and so on.^{29,31} Their outstanding aggregation capability enables them to act as templates or crystal growth modifiers in the nucleation and growth stages. Using gemini surfactants, various noble metal nanomaterials, including spherical nanoparticles,³² nanorods/nanowires,^{33,34} nanoribbons³⁵ as well as nanoflowers,³⁶ have been fabricated. However, the construction of 2DHBNs with gemini surfactants has not yet been reported.

Herein, we demonstrate a facile method for the controlled synthesis of 2DHBNs with the assistance of the cationic gemini surfactant hexamethylene-1,6-bis (dodecyl dimethylammonium bromide) ($C_{12}C_6C_{12}Br_2$). Systematic studies were performed to investigate the formation of the branched nanostructures and a possible mechanism has been proposed.

Experimental section

Materials and methods

Chloroauric acid ($HAuCl_4 \cdot 4H_2O$, 99.9%) was purchased from Shenyang Jinke Reagents Plant. Ascorbic acid (AA) of analytical grade was obtained from Sinopharm Chemical Reagent Co., Ltd. Rhodamine 6G (R6G) was purchased from Aldrich. The gemini surfactant $C_{12}C_6C_{12}Br_2$ was synthesized as reported³⁷ and was used after repeated recrystallization. Milli-Q deionized water (18 M Ω cm) was used to prepare all the solutions.

As a typical procedure, 8 μ L of a $C_{12}C_6C_{12}Br_2$ solution (100 mM) and 66.7 μ L of a $HAuCl_4$ aqueous solution (24 mM) was added into 9 mL of water in sequence and mixed. After that, 32 μ L of freshly prepared AA (50 mM) was rapidly injected into the above mixture with vigorous stirring for 30 s and the reaction mixture was kept at 25 $^\circ$ C under static conditions for at least 1 h. Upon adding AA, the color of the reaction solution immediately changed from dark yellow to colorless, suggesting the reduction of Au(III) to the Au(I) species. The color of the solution then gradually changed from colorless to brown with time, indicating the formation of gold nanoparticles. The product was collected by centrifugation at 3000 rpm for 5 min. Subsequently, the supernatant was removed and pure water was added to the precipitate. The residue was dispersed by sonication for 5 min. The rinsing procedure was repeated at least three times to obtain the final gold nanomaterials.

Characterization of the gold nanostructures

The obtained gold products were characterized by scanning electron microscopy (SEM, Hitachi S-4800, 10 kV), transmission electron microscopy (TEM, JEM-1011, 100 kV), high resolution TEM (HRTEM, JEM-2100, 200 kV) and X-ray diffraction (XRD, Rigaku D/max-2500, Cu-K α radiation, 40 kV, 200 mA). SEM and TEM specimens were prepared by placing one drop of the aqueous dispersion of the gold product on a silicon wafer and a carbon-coated copper grid, respectively, allowing water to evaporate at ambient temperature. For the XRD measurements, the gold product aqueous dispersion was dropped onto a glass slide and allowed to dry naturally in the air.

SERS measurements

For the SERS measurements, R6G was used as a probe molecule. The SERS substrate was prepared by drop-casting 20 μ L of 2DHBN dispersions on a 0.5 cm \times 0.5 cm silica wafer and allowing to dry in the atmosphere. Then, 10 μ L of a R6G ethanol solution (10^{-6} M) was spread onto the prepared gold substrate. SERS measurements were carried out on a Renishaw inVia Plus Raman microscope with excitation from a 785 nm laser in one scan. The laser power was 10 mW. Spectra were collected by focusing the laser beam onto the sample using a 50 \times objective, providing a spatial resolution of approximately 1 μ m. The data acquisition time was 50 s for one accumulation. To test the reproducibility, measurements were performed at different positions on each sample.

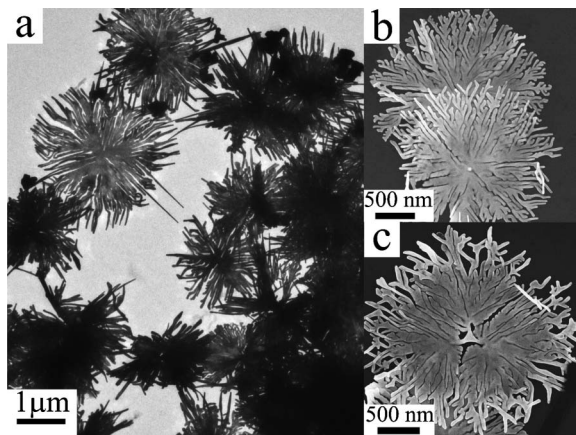


Fig. 1 TEM (a) and SEM (b, c) images of the obtained 2DHBNs from the reduction of 0.2 mM HAuCl₄ by 0.2 mM AA in the presence of 0.1 mM C₁₂C₆C₁₂Br₂.

Results and discussion

Characterization of the 2DHBNs

A special kind of gold nanostructure, snowflake-like 2DHBNs, was obtained by adding AA to a solution of 0.1 mM C₁₂C₆C₁₂Br₂ and 0.2 mM HAuCl₄. Fig. 1a shows the low magnification TEM image of the 2DHBNs composed of many nanoarms, which are grown from a core in a radial fashion.

The diameter of the 2DHBNs is *ca.* 3 μm. Two types of 2DHBNs are found, differentiating in the shapes of their cores. One adopts a quasi-circular core (Fig. 1b) and the other adopts a distinct triangular nanoprism core (Fig. 1c). Although the microscope observation cannot show the exact statistical yields of the two types of products due to the superposition of some 2DHBNs, the 2DHBNs with nummular cores are obviously more dominant.

To obtain the crystallographic structure information, XRD and HRTEM measurements were employed. As illustrated in Fig. 2a, the XRD pattern of the 2DHBNs exhibits five sharp diffraction peaks exclusively ascribed to gold crystals with a face-centered-cubic (fcc) structure, indicating that the 2DHBNs are pure, well-crystallized gold crystals. Fig. 2b is a representative TEM image of an individual 2DHBN lying on a copper grid and the region marked with a white frame was selected to carry out electron diffraction (ED) and HRTEM observations. The ED pattern (Fig. 2c) shows the formally forbidden $(1/3)\{422\}$ reflections, which can be indexed to the $[\bar{1}11]$ zone axis of the fcc gold, indicating that the arm grows along the $\langle 211 \rangle$ direction and with the (111) plane as the top surface. The related HRTEM image (Fig. 2d) exhibits clear lattice fringes with a *d* spacing of 0.24 nm, which can be ascribed to the $3 \times \{422\}$ superlattice spacing of the fcc gold crystals, confirming that the arm grows along the $\langle 211 \rangle$ direction. Other arms of the 2DHBN also grow along the $\langle 211 \rangle$ direction, as confirmed by HRTEM (Fig. S1, ESI†), indicating that the 2DHBNs are uniform in crystallographic orientation.

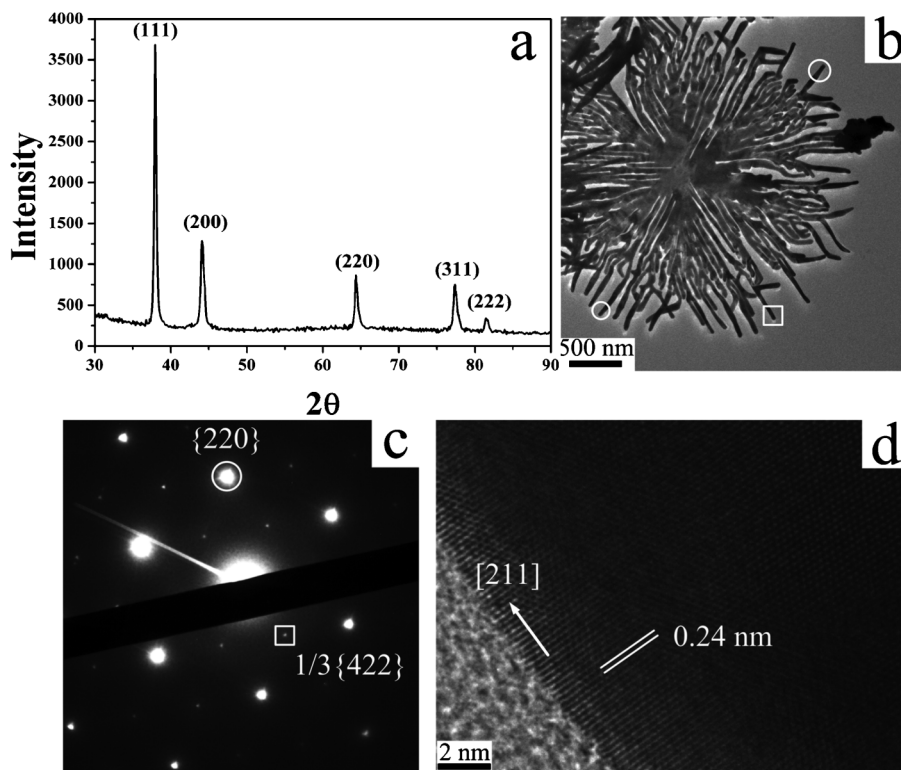


Fig. 2 XRD pattern of the 2DHBNs (a), TEM image of a representative 2DHBN (b), SAED pattern (c) and HRTEM image (d) of the tip of an arm, as marked by a white frame in panel b.

Furthermore, it should be pointed out that the appearance of the forbidden spots of the $1/3\{422\}$ diffractions normally suggests that at least one stacking fault or twin plane exists in the (111) plane perpendicular to the electron beam.³⁸ The HRTEM image of a single arm perpendicular to the TEM grid clearly shows the (111) twin planes, indicating that the 2DHBNs are twin crystals (Fig. S2, ESI†). On the basis of these analyses, it can be concluded that the 2DHBNs grow along the $\langle 211 \rangle$ direction and present multiple twin planes stacked along the $\langle 111 \rangle$ direction.

Time dependent growth of 2DHBNs

As mentioned above, a small amount of the 2DHBNs have a triangular prism core, which implies that the nanostructure may be generated by overgrowth from the triangular prism. In order to confirm this hypothesis, the products from different reaction times were isolated and characterized by TEM. The reaction times were shortened to 2, 5, 10 and 30 min and the TEM images of the typical gold nanoparticles formed are shown in Fig. 3. The low magnification SEM images of the nanoparticles obtained at different reaction times are shown in Fig. S3, ESI†

At the beginning of the reaction (2 min), typical triangular nanoprisms formed (Fig. 3a) and premature tripods with a distinct 3-fold symmetry evolved from the triangular nanopr-

isms (Fig. 3b), indicating that the branched growth starts from the tips of the nanoprism. The triangular nanoprism grew into matured tripods with three long arms within 5 min (Fig. 3c). Interestingly, the second generation overgrowth from the arms was also displayed in the products collected at 5 min (Fig. 3d). The multi-generation overgrowth was observed after a reaction time of 10 min (Fig. 3e). At 30 min, the structure turned into complete snowflake-like 2DHBNs with a triangular nanoprism central core (Fig. 3f). However, more of the final 2DHBNs display a nummular core rather than a triangular prism (Fig. 3g), which may be related to the inordinate overgrowth and arm fusions (Ostwald ripening). In this case, the overgrowth occurred both at the tips and the edges of the triangular nanoprism (Fig. S4, ESI†) and the crowded arms fused with each other, tending to develop into a nummular core. It is therefore concluded that the multi-generation branching growth from the triangular prism core gives birth to a highly branched nanostructure.

HRTEM measurements were applied to investigate the overgrowth direction of the above nanostructures. The results for a typical intermediate of the 2DHBNs are shown in Fig. 4. The appearance of the hexagonal diffraction from the $\{220\}$ and $\{422\}$ planes with the zone axis along the $\langle 111 \rangle$ direction (Fig. 3b–d) and the $3 \times \{422\}$ superlattice spacing of the fcc gold (Fig. 4e and f) indicates that the intermediate adopts the (111) plane as the top surface and the branched arms grow from the $\langle 211 \rangle$ direction.

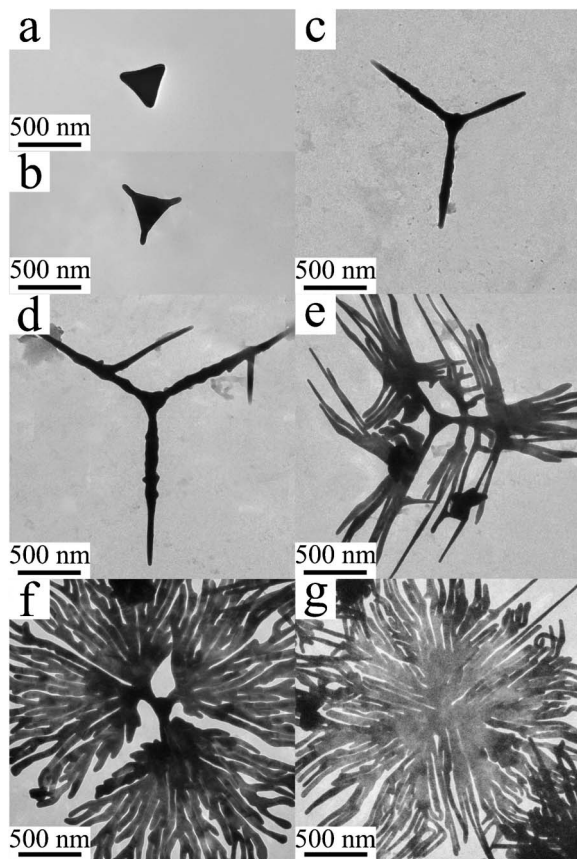


Fig. 3 TEM images of the gold products obtained after a reaction time of 2 min (a, b), 5 min (c, d), 10 min (e) and 30 min (f, g). $[C_{12}C_6C_{12}Br_2] = 0.1$ mM, $[HAuCl_4] = 0.2$ mM, $[AA] = 0.2$ mM, $25^\circ C$.

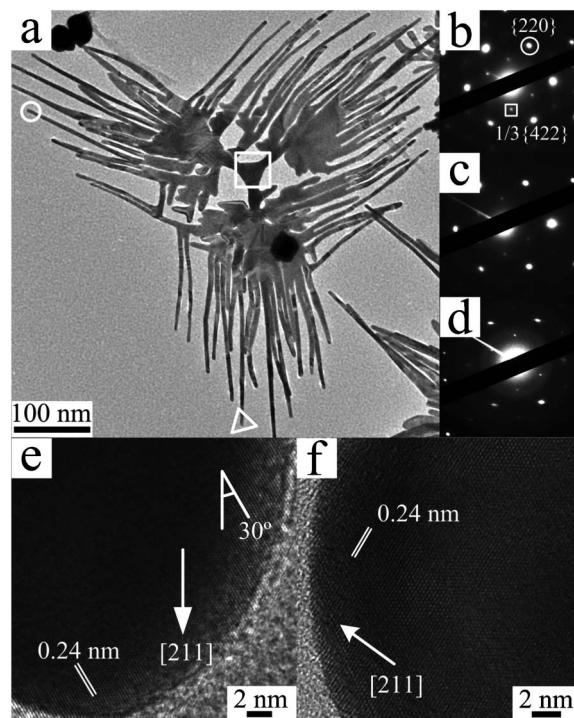


Fig. 4 TEM image for a typical intermediate of the 2DHBNs formed after a reaction time of 10 min (a), the ED patterns of the regions marked by the white square (b), triangle (c) and circle (d), and the HRTEM images of the related region marked by a triangle (e) and circle (f).

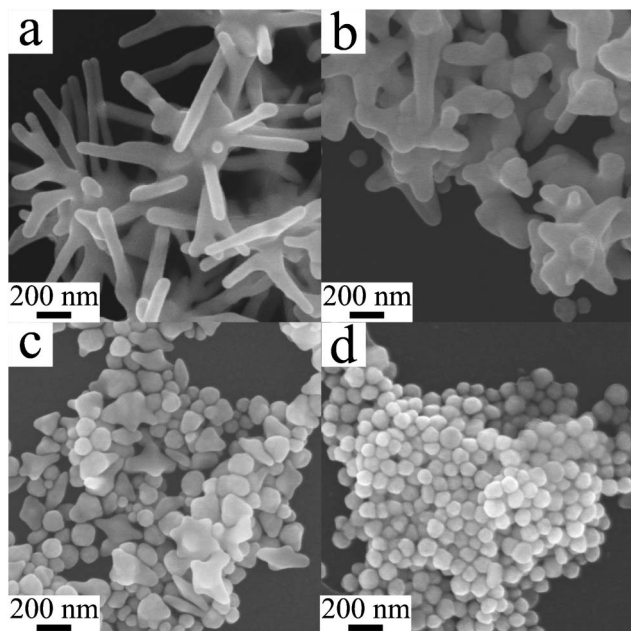


Fig. 5 Influence of the reaction temperature on branched Au nanocrystal formation: 30 °C (a), 40 °C (b), 50 °C (c) and 60 °C (d). $[C_{12}C_6C_{12}Br_2] = 0.1$ mM, $[HAuCl_4] = 0.2$ mM, $[AA] = 0.2$ mM.

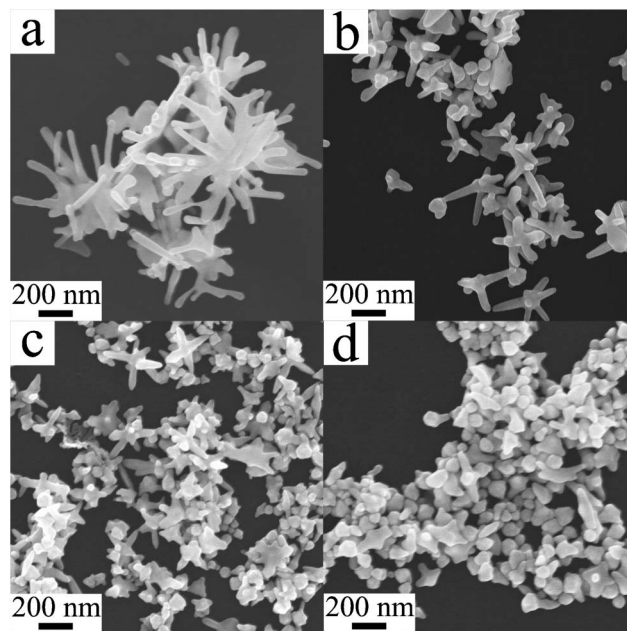


Fig. 6 Influence of AA concentration on the branched gold products formation at 25 °C: 0.3 mM (a), 0.4 mM (b), 1 mM (c) and 2 mM (d). $[C_{12}C_6C_{12}Br_2] = 0.1$ mM, $[HAuCl_4] = 0.2$ mM.

Effect of reaction temperature and AA concentration

Previous studies^{18,24} have demonstrated that branched growth is driven by kinetic factors due to the highly symmetrical crystalline structures of the fcc crystal. To investigate the influence of the growth kinetics on the formation of the present 2DHBNs, the reaction temperature was varied from 25 °C to 60 °C. Fig. 5 shows the effect of the reaction temperature on the morphology of the as-prepared gold nanoparticles. As illustrated in Fig. 1, 2DHBNs were formed at 25 °C. If the temperature was increased to 30 °C, the product transformed into three-dimensional highly branched nanostructures with coral-like morphology (Fig. 5a). Further increasing the reaction temperature to 40 or 50 °C led to a remarkable decrease in the length and number of arms (Fig. 5b and c). When the temperature was increased to 60 °C, quasi-spherical nanoparticles were dominantly generated (Fig. 5d). In brief, the gold products with the most extended and branched features were generated at a temperature below 30 °C. Notably, a higher temperature inhibits the branched growth of the gold nanocrystal. The tendency to minimize the surface energy is a determining factor to the shape of the nanoparticles. Spherical or polyhedral nanoparticles with a low surface energy are favored compared with branched nanostructures. The formation of the equilibrium shape normally requires fast kinetics. In the present situation, the branching degree of the gold products decreases on raising the temperature. This means that a higher temperature leads to faster growth of the nanostructures, benefiting the formation of spherical nanoparticles with a low surface energy.

The influence of the growth kinetics on the formation of gold nanocrystals was also studied by changing the reducing agent concentration. Fig. 6 shows the effect of the AA

concentration on the morphology of the formed gold nanoparticles. An obvious change of the product morphology from highly branched nanostructures to irregular nanostars with several tips can be observed with the increase of the AA concentration. Clearly, the fast reduction rate blocks the branched growth of gold nanocrystals. Branched nanostructures with a higher surface energy are kinetically-controlled products and their formation requires that the rate of atomic addition to the nucleated nanocrystal is greater than the subsequent surface adatom diffusion otherwise stable shapes, such as polyhedra, will form through adatom diffusion on the surface of the growing nanocrystals.^{18,39} Herein, at high concentrations of AA, a large number of nuclei form due to the high reduction rate of the gold ions. The remaining gold ions are significantly depleted by nucleation events. As a result, the generation rate of adatoms is restricted and thus the low concentration of adatoms per nucleated nanocrystal makes the overgrowth unfavorable.

Effect of $C_{12}C_6C_{12}Br_2$ concentration

To clarify the role of $C_{12}C_6C_{12}Br_2$, control experiments were performed in the absence of $C_{12}C_6C_{12}Br_2$ and in the presence of $C_{12}C_6C_{12}Br_2$ with various concentrations, at a constant concentration of $HAuCl_4$ and AA. As shown in Fig. 7a, only polyhedral gold nanoparticles were obtained without $C_{12}C_6C_{12}Br_2$. In the solution containing 0.05 mM $C_{12}C_6C_{12}Br_2$, irregular nanoparticles together with a small amount of plate-like nanoparticles were formed (Fig. 7b). When the $C_{12}C_6C_{12}Br_2$ concentration increased to 0.1 mM, the products changed into the aforementioned 2DHBNs (Fig. 1). However, on further increasing the $C_{12}C_6C_{12}Br_2$ concentration to 0.2 mM or higher, branched growth was inhibited and

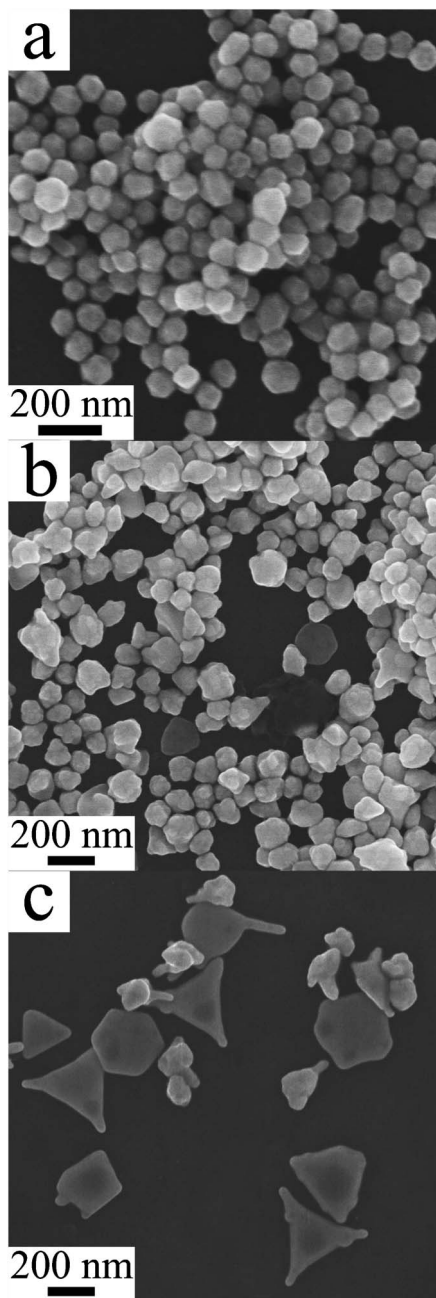


Fig. 7 Influence of the $C_{12}C_6C_{12}Br_2$ concentration on the formation of branched gold products at 25 °C: 0 mM (a), 0.05 mM (b) and 0.2 mM (c). $[HAuCl_4] = 0.2$ mM, $[AA] = 0.2$ mM.

triangular nanoprisms with short arms and irregular nanoparticles were formed (Fig. 7c). The product morphology was stagnated at the initial stage of the 2DHBNS, indicating that the kinetic factor plays an important role. In fact, the reaction rate was extremely decelerated in the 0.2 mM $C_{12}C_6C_{12}Br_2$ solution, where no gold nanostructures were observed within 6 h and only a small amount of gold nanoparticles could be collected after 12 h.

To better understand the growth kinetics related to the $C_{12}C_6C_{12}Br_2$ concentration, time-dependent UV-vis absorbance

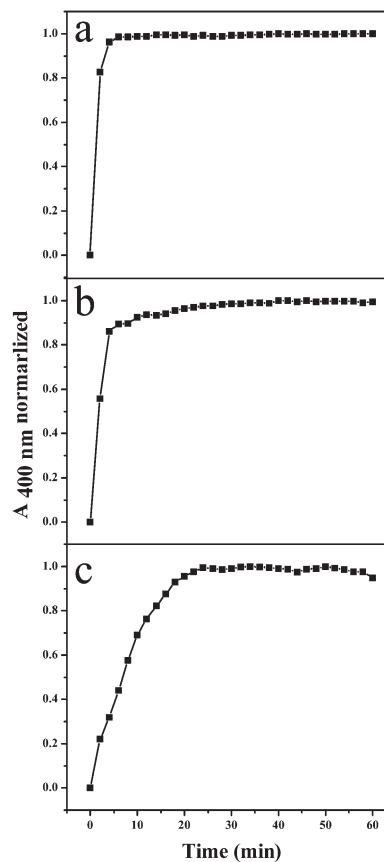


Fig. 8 The plot of $A_{400\text{ nm}}$ versus time for the reaction solutions with different $C_{12}C_6C_{12}Br_2$ concentrations: 0 mM (a), 0.05 mM (b) and 0.10 mM (c).

spectra were applied to monitor the reaction process. The typical UV-vis absorption spectra of the 2DHBNS are shown in Fig. S5, ESI†. The absorbance at 400 nm ($A_{400\text{ nm}}$) can be used as an indication of the amount of metallic gold present in the sample.⁴⁰ Fig. 8 shows the evolution of $A_{400\text{ nm}}$ as a function of time. In the absence of $C_{12}C_6C_{12}Br_2$, $A_{400\text{ nm}}$ significantly increased and almost remained constant after 6 min (Fig. 8a). In the presence of 0.05 mM $C_{12}C_6C_{12}Br_2$, the $A_{400\text{ nm}}$ dramatically increased in the first 4 min and then reached a plateau within 20 min (Fig. 8b). When 0.1 mM $C_{12}C_6C_{12}Br_2$ was used, different growth characteristics appeared (Fig. 8c). $A_{400\text{ nm}}$ steadily increased within 18 min and then the slope decreased and reached a plateau. As to the solution containing a higher concentration of $C_{12}C_6C_{12}Br_2$, UV-vis absorbance spectra were not suitable for monitoring the growth kinetics anymore because large vesicles formed after the addition of AA which led to an intense absorption around 400 nm. The formation of the vesicles was confirmed by DLS and TEM characterizations (Fig. S6, ESI†).

Apart from the kinetics effect, $C_{12}C_6C_{12}Br_2$ also acts as a capping agent, which plays an important role in the final morphology of the gold products. When $C_{12}C_6C_{12}Br_2$ was replaced by the corresponding single chain surfactant dodecyltrimethylammonium bromide (DTAB), only irregular particles were observed in the product (Fig. S7, ESI†). Qi and co-

workers^{23b} obtained a similar irregular product in DTAB/HAuCl₄/AA, and found that if β -CD was introduced, the DTAB/ β -CD inclusion complexes could selectively adsorb onto the gold (111) planes to give a 2D nanodendrite. This study indicates that molecule structures could greatly influence the adsorption selectivity of surfactants. Herein, the C₁₂C₆C₁₂Br₂ molecules may selectively anchor onto the (111) planes, facilitating the formation of 2D nanostructures with the exposed (111) plane as the top surface.

Possible formation mechanism of the 2DHBNs

On the basis of the results and discussions above, the possible formation mechanism of the 2DHBNs is proposed as follows. The process of the formation of 2DHBNs can be roughly divided into two stages. The first stage involves the reduction of Au(III) to Au(I) and then to Au(0) in the form of the triangular nanoprisms. The second stage involves the radical overgrowth along the <211> direction from the center of the triangular nanoprism through the autocatalytic reduction of Au(I) on the surface.

C₁₂C₆C₁₂Br₂ is indispensable for the construction of 2DHBNs. The possible roles of C₁₂C₆C₁₂Br₂ can be described as (i) a capping agent and (ii) a kinetics controller. Acting as a capping agent, C₁₂C₆C₁₂Br₂ may selectively adsorb onto the (111) planes so that the 2D nanostructures are generated. Acting as a kinetics controller, the quaternary ammonium cations of C₁₂C₆C₁₂Br₂ can bind with both Au(III) and Au(I) through strong electrostatic interactions and thereby lead to a decrease in the reduction potential of the gold ions and a decrease in the diffusion rate of the gold ions. In particular, C₁₂C₆C₁₂Br₂ carries two charges and two hydrocarbon chains and thus the binding of the gemini surfactant with the gold precursor can reduce the diffusion rate of the gold ions to a greater extent than the corresponding single chain surfactants. As a result, C₁₂C₆C₁₂Br₂ can significantly influence the nucleation and growth process. That is to say, the C₁₂C₆C₁₂Br₂ concentration must be high enough in order to yield the 2DHBNs. If the concentration of C₁₂C₆C₁₂Br₂ is too low, extra gold ions cannot bind with C₁₂C₆C₁₂Br₂ and the resultant rapid reduction rate will generate irregular nanoparticles.

On the other hand, the present overgrowth of gold nanostructures is an autocatalytic reaction. As reported,²⁸ the collision frequency of gold ions with nucleated nanocrystals is another important factor which affects the growth rate. Therefore, the difference in the diffusion rate between the complexes of the gemini surfactant with the gold precursor and the aggregates formed by the complexes should be considered. The diffusion rate of larger aggregates should be less than for smaller aggregates, inversely proportional to the weight of the aggregates. Consequently, the large aggregates should have a lower collision frequency to the nucleated nanocrystals and significantly lower the growth rate of the nanostructures, which will inhibit the generation of 2DHBNs, just as the gold morphology was stagnated at the initial stage of the 2DHBNs when large vesicles of C₁₂C₆C₁₂Br₂ (0.2 mM) were applied.

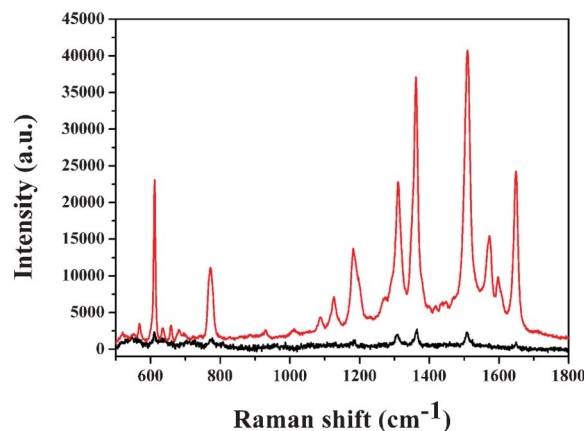


Fig. 9 Raman spectrum of solid R6G and the SERS spectrum of R6G adsorbed onto the 2DHBNs.

SERS activity of 2DHBNs

Previous studies⁴¹ demonstrate that gold branched nanostructures present a great deal of sharp corners, edges and junctions, which act as electromagnetic hot spots for SERS. Herein, the SERS sensitivity of the as-prepared 2DHBNs was investigated using R6G as a model molecule. Fig. 9 shows the Raman spectra of solid R6G and the SERS spectra of 1×10^{-6} M R6G adsorbed onto a 2DHBN-decorated substrate. Only several very weak Raman signals were presented in the spectrum of the solid R6G, while extremely strong Raman signals were clearly observed in the SERS spectrum. The pronounced Raman peaks are in agreement with previous work,^{42,43} which can be ascribed to the C–C stretching of the xanthenes ring (1650, 1572, 1510, 1362 cm⁻¹), C–O–C stretching (1312 cm⁻¹), C–H in-plane bending (1183 cm⁻¹), C–H out-of-plane bending (773 cm⁻¹), and C–C–C ring in-plane bending (611 cm⁻¹). The average calculated enhanced factor (EF)⁴⁴ for the R6G is 6.29×10^5 (ESI†). This strongly enhanced effect indicates that the as-prepared 2DHBNs could be used as an effective SERS substrate for many potential applications.

Conclusions

Snowflake-like 2DHBNs grown along the <211> direction have been fabricated using the cationic ammonium gemini surfactant C₁₂C₆C₁₂Br₂. The gemini surfactant is not only a capping agent but also as a kinetics controller in the formation of the 2DHBNs. C₁₂C₆C₁₂Br₂ molecules may prefer to adsorb onto the (111) planes, promoting the generation of the 2D nanostructures. Moreover, the binding of C₁₂C₆C₁₂Br₂ molecules with gold ions leads to a decrease in the reduction potential of the gold ions and a decrease in the diffusion rate of the gold ions. When the C₁₂C₆C₁₂Br₂ concentration is high enough, the collision frequency of the gold ions to the nucleated nanocrystals can be greatly decreased by the large vesicles formed with the complexes and in turn the growth rate of the nanostructures can be lowered. As a result, the growth rate decreases with an increase in the C₁₂C₆C₁₂Br₂ concentra-

tion and well-defined 2DHBNs are generated. The as-prepared 2DHBNs show a high SERS activity and have potential application in SERS based detection and other nano-devices. Due to the special adsorption and aggregation properties of gemini surfactants, it is anticipated that novel nanostructures of other noble metals can be synthesized using gemini surfactants.

Acknowledgements

We are grateful for the financial support from National Natural Science Foundation of China (21025313, 21021003).

References

- (a) W. F. Smith, *Nat. Nanotechnol.*, 2007, **2**, 77; (b) L. Bürgi, N. Knorr, H. Brune, M. A. Schneider and K. Kern, *Appl. Phys. A: Mater. Sci. Process.*, 2002, **75**, 141.
- (a) M. Rycenga, C. M. Cobley, J. Zeng, W. Li, C. H. Moran, Q. Zhang, D. Qin and Y. Xia, *Chem. Rev.*, 2011, **111**, 3669; (b) R. Jin, Y. Cao, C. A. Mirkin, K. L. Kelly, G. C. Schatz and J. G. Zheng, *Science*, 2001, **294**, 1901; (c) R. Jin, Y. Cao, E. Hao, G. S. Métraux, G. C. Schatz and C. A. Mirkin, *Nature*, 2003, **425**, 487; (d) K. L. Shuford, M. A. Ratner and G. C. Schatz, *J. Chem. Phys.*, 2005, **123**, 114713.
- M. G. Blaber, A.-I. Henry, J. M. Bingham, G. C. Schatz and R. P. van Duyne, *J. Phys. Chem. C*, 2012, **116**, 393.
- A. J. Haes and R. P. van Duyne, *J. Am. Chem. Soc.*, 2002, **124**, 10596.
- J. Y. Kim and J. S. Lee, *Chem. Mater.*, 2010, **22**, 6684.
- K. Imura, T. Nagahara and H. Okamoto, *Appl. Phys. Lett.*, 2006, **88**, 023104.
- (a) R. Baigorri, J. M. García-Mina, R. F. Aroca and R. A. Alvarez-Puebla, *Chem. Mater.*, 2008, **20**, 1516; (b) K. A. Stoerzinger, J. Y. Linb and T. W. Odom, *Chem. Sci.*, 2011, **2**, 1435.
- (a) L. N. Lewis, *Chem. Rev.*, 1993, **93**, 2693; (b) R. N. Goyal, A. A. Umar and M. J. Oyama, *J. Electroanal. Chem.*, 2009, **631**, 58; (c) J. X. Wang, N. M. Markovic and R. R. Adzic, *J. Phys. Chem. B*, 2004, **108**, 4127.
- (a) X. Liu, N. Wu, B. H. Wunsch, R. J. Barsotti Jr and F. Stellacci, *Small*, 2006, **2**, 1046; (b) L. Lu, A. Kobayashi, K. Tawa and Y. Ozaki, *Chem. Mater.*, 2006, **18**, 4894; (c) K. Imura, T. Nagahara and H. Okamoto, *Appl. Phys. Lett.*, 2006, **88**, 23104; (d) S. S. Shankar, A. Rai, B. Ankamwar, A. Singh, A. Ahmad and M. Sastry, *Nat. Mater.*, 2004, **3**, 482.
- (a) J. E. Millstone, G. S. Métraux and C. A. Mirkin, *Adv. Funct. Mater.*, 2006, **16**, 1209; (b) V. Bastys, I. Pastoriza-Santos, B. Rodríguez-González, R. Vaisnoras and L. M. Liz-Marzan, *Adv. Funct. Mater.*, 2006, **16**, 766; (c) W. Huang, W. Qian and M. A. El-Sayed, *J. Appl. Phys.*, 2005, **98**, 114301; (d) C. Xue and C. A. Mirkin, *Angew. Chem., Int. Ed.*, 2007, **46**, 2036.
- M. Maillard, P. Huang and L. Brus, *Nano Lett.*, 2003, **3**, 1611.
- (a) T. Tsuruoka, C. H. Liang, K. Terabe and T. Hasegawa, *Appl. Phys. Lett.*, 2008, **92**, 091908; (b) X. Y. Kong and Z. L. Wang, *Nano Lett.*, 2003, **3**, 1625; (c) M. S. Arnold, P. Avouris, Z. W. Pan and Z. L. Wang, *J. Phys. Chem. B*, 2003, **107**, 659; (d) Z. W. Pan, Z. R. Dai and Z. L. Wang, *Science*, 2001, **291**, 1947.
- Y. Song, Y. Yang, C. J. Medforth, E. Pereira, A. K. Singh, H. Xu, Y. Jiang, C. J. Brinker, F. van Swol and J. A. Shelnutt, *J. Am. Chem. Soc.*, 2004, **126**, 635.
- A. Swami, M. Kasture, R. Pasricha and M. Sastry, *J. Mater. Chem.*, 2004, **14**, 709.
- K. Jasuja and V. Berry, *ACS Nano*, 2009, **3**, 2358.
- A. Gutes, C. Carraro and R. Maboudian, *J. Am. Chem. Soc.*, 2010, **132**, 1476.
- Y. Ding, M. Chen and J. Erlebacher, *J. Am. Chem. Soc.*, 2004, **126**, 6876.
- B. Lim and Y. Xia, *Angew. Chem., Int. Ed.*, 2010, **50**, 76.
- X. T. Bai and L. Q. Zheng, *Cryst. Growth Des.*, 2010, **10**, 4701.
- T. Shtoyko, E. G. Matveeva, I.-F. Chang, Z. Gryczynski, E. Goldys and I. Gryczynski, *Anal. Chem.*, 2008, **80**, 1962.
- M. Pan, H. Sun, J. W. Lim, S. R. Bakaul, Y. Zeng, S. Xing, T. Wu, Q. Yan and H. Chen, *Chem. Commun.*, 2012, **48**, 1440.
- S. Chen, Z. L. Wang, J. Ballato, S. H. Foulger and D. L. Carroll, *J. Am. Chem. Soc.*, 2003, **125**, 16186.
- (a) N. Zhao, Y. Wei, N. Sun, Q. Chen, J. Bai, L. Zhou, Y. Qin, M. Li and L. Qi, *Langmuir*, 2008, **24**, 991; (b) T. Huang, F. Meng and L. Qi, *Langmuir*, 2010, **26**, 7582.
- J. Watt, S. Cheong, M. F. Toney, B. Ingham, J. Cookson, P. T. Bishop and R. D. Tilley, *ACS Nano*, 2010, **4**, 396.
- C. J. Murphy, T. K. Sau, A. M. Gole, C. J. Orendorff, J. Gao, L. Gou, S. E. Hunyadi and T. Li, *J. Phys. Chem. B*, 2005, **109**, 13857.
- Y. Xia, Y. Xiong, B. Lim and S. E. Skrabalak, *Angew. Chem., Int. Ed.*, 2009, **48**, 60.
- J. Xiao and L. Qi, *Nanoscale*, 2011, **3**, 1383.
- J. Pérez-Juste, L. M. Liz-Marzán, S. Carnie, D. Y. C. Chan and P. Mulvaney, *Adv. Funct. Mater.*, 2004, **14**, 571.
- (a) R. Zana, *Adv. Colloid Interface Sci.*, 2002, **97**, 203; (b) F. M. Menger and J. S. Keiper, *Angew. Chem., Int. Ed.*, 2000, **39**, 1906.
- M. S. Bakshi, *Langmuir*, 2009, **25**, 12697.
- (a) G. Bai, J. Wang, H. Yan, Z. Li and R. K. Thomas, *J. Phys. Chem. B*, 2001, **105**, 3105; (b) S. D. Wettig and R. E. Verrall, *J. Colloid Interface Sci.*, 2001, **244**, 377; (c) A. Kanaebal, R. Oda, E. Mendes and S. J. Candau, *Langmuir*, 2000, **16**, 2493.
- (a) Q. Liu, M. Guo, Z. Nie, J. Yuan, J. Tan and S. Yao, *Langmuir*, 2008, **24**, 1595; (b) M. S. Bakshi, P. Sharma, T. S. Banipal, G. Kaur, K. Torigoe, N. O. Petersen and F. Possmayer, *J. Nanosci. Nanotechnol.*, 2007, **7**, 916; (c) L. Casal-Dujat, M. Rodrigues, A. Yagüe, A. C. Calpena, D. B. Amabilino, J. González-Linares, M. Borràs and L. Pérez-García, *Langmuir*, 2012, **28**, 2368; (d) J. Xu, X. Han, H. Liu and Y. Hu, *J. Dispersion Sci. Technol.*, 2005, **26**, 473.
- (a) A. Guerrero-Martínez, J. Pérez-Juste, E. Carbó-Argibay, G. Tardajos and L. M. Liz-Marzán, *Angew. Chem., Int. Ed.*, 2009, **48**, 9484; (b) S. Bhattacharya and J. Biswas, *Nanoscale*, 2011, **3**, 2924.
- (a) K. Esumi, J. Hara, N. Aihara, K. Usui and K. Torigoe, *J. Colloid Interface Sci.*, 1998, **208**, 578; (b) J. Xu, J. Hu, C. Peng, H. Liu and Y. Hu, *J. Colloid Interface Sci.*, 2006,

- 298, 689; (c) L. Zhong, T. Jiao and M. Liu, *Langmuir*, 2008, **24**, 11677.
- 35 M. S. Bakshi, F. Possmayer and N. O. Petersen, *J. Phys. Chem. C*, 2008, **112**, 8259.
- 36 L. Zhong, X. Zhai, X. Zhu, P. Yao and M. Liu, *Langmuir*, 2010, **26**, 5876.
- 37 R. Zana, M. Benrraou and R. Rueff, *Langmuir*, 1991, **7**, 1072.
- 38 (a) A. I. Kirkland, D. A. Jefferson, D. G. Duff, P. P. Edwards, I. Gameson, B. F. G. Johnson and D. J. Smith, *Proc. R. Soc. London, Ser. A*, 1993, **440**, 589; (b) V. Germain, J. Li, D. Ingert, Z. L. Wang and M. P. Pileni, *J. Phys. Chem. B*, 2003, **107**, 8717; (c) C. Salzemann, J. Urban, I. Lisiecki and M. P. Pileni, *Adv. Funct. Mater.*, 2005, **15**, 1277; (d) S. Maksimuk, X. Teng and H. Yang, *J. Phys. Chem. C*, 2007, **111**, 14312.
- 39 (a) N. Ortiz and S. E. Skrabalak, *Cryst. Growth Des.*, 2011, **11**, 3545; (b) J. Li, J. Wu, X. Zhang, Y. Liu, D. Zhou, H. Sun, H. Zhang and B. Yang, *J. Phys. Chem. C*, 2011, **115**, 3630; (c) E. Dinda, M. H. Rashid and T. K. Mandal, *Cryst. Growth Des.*, 2010, **10**, 2421; (d) Y. Lee and T. G. Park, *Langmuir*, 2011, **27**, 2965; (e) B. Viswanath, P. Kundu, A. Halder and N. Ravishankar, *J. Phys. Chem. C*, 2009, **113**, 16866.
- 40 P. C. Angelomé, H. H. Mezerji, B. Goris, I. Pastoriza-Santos, J. Pérez-Juste, S. Bals and L. M. Liz-Marzán, *Chem. Mater.*, 2012, **24**, 1393.
- 41 R. A. Alvarez-Puebla and L. M. Liz-Marzán, *Chem. Soc. Rev.*, 2012, **41**, 43.
- 42 J. Fang, S. Du, S. Lebedkin, Z. Li, R. Kruk, M. Kappes and H. Hahn, *Nano Lett.*, 2010, **10**, 5006.
- 43 P. Hildebrandt and M. Stockburger, *J. Phys. Chem.*, 1984, **88**, 5935.
- 44 (a) S. Guo, S. Dong and E. Wang, *Cryst. Growth Des.*, 2008, **9**, 372; (b) X. Bai, Y. Gao and L. Zheng, *CrystEngComm*, 2011, **13**, 3562.